



# Observation of an optical vortex beam from a helical undulator in the XUV region

Tatsuo Kaneyasu,<sup>a\*</sup> Yasumasa Hikosaka,<sup>b</sup> Masaki Fujimoto,<sup>c,d</sup> Hiroshi Iwayama,<sup>c,d</sup> Masahito Hosaka,<sup>e</sup> Eiji Shigemasa<sup>c,d</sup> and Masahiro Katoh<sup>c,d</sup>

<sup>a</sup>Saga Light Source, Tosu 841-0005, Japan, <sup>b</sup>Graduate School of Medicine and Pharmaceutical Sciences, University of Toyama, Toyama 930-0194, Japan, <sup>c</sup>UVSOR Facility, Institute for Molecular Science, Okazaki 444-8585, Japan, <sup>d</sup>Sokendai (The Graduate University for Advanced Studies), Okazaki 444-8585, Japan, and <sup>e</sup>Synchrotron Radiation Research Center, Nagoya University, Nagoya 464-0824, Japan. \*Correspondence e-mail: kaneyasu@saga-ls.jp

Received 8 June 2017

Accepted 29 June 2017

Edited by M. Eriksson, Lund University, Sweden

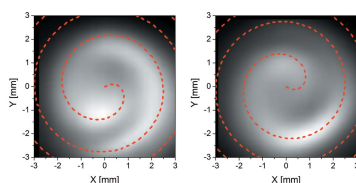
**Keywords:** XUV vortex; helical undulator radiation; interference.

The observation of an optical vortex beam at 60 nm wavelength, produced as the second-harmonic radiation from a helical undulator, is reported. The helical wavefront of the optical vortex beam was verified by measuring the interference pattern between the vortex beam from a helical undulator and a normal beam from another undulator. Although the interference patterns were slightly blurred owing to the relatively large electron beam emittance, it was possible to observe the interference features thanks to the helical wavefront of the vortex beam. The experimental results were well reproduced by simulation.

## 1. Introduction

An optical vortex beam carries orbital angular momentum (OAM), as well as spin angular momentum, associated with its circular polarization. Since the theoretical demonstration of the OAM carried by a Laguerre–Gaussian mode beam (Allen *et al.*, 1992), there has been an increasing number of studies on optical vortices in a wide range of research fields, such as microscopy (Hell, 2003), astrophysics (Harwit, 2003), manipulation of small particles (Padgett & Bowman, 2011) and laser ablation (Omatsu *et al.*, 2010). The radiation field of the optical vortex is characterized by the phase term  $\exp(il\varphi)$ , where  $\varphi$  is the azimuthal angle around the propagation axis, and the well defined OAM  $l\hbar$  is carried by each photon. Because of the existence of phase singularity, the vortex beam has a dark center in its cross section where the field intensity vanishes. In the last few decades, most studies using an optical vortex beam have been conducted in the visible region because a helically phased beam is readily obtained from a Gaussian beam using optical elements, such as a spiral-phase plate (Beijersbergen *et al.*, 1994), computer-generated hologram (Heckenberg *et al.*, 1992) or q-plate (Marrucci *et al.*, 2006).

Recently, it has been reported that the spiral motion of a relativistic electron naturally leads to the emission of photons carrying OAM (Katoh *et al.*, 2017a). A typical example of vortex radiation is found in the harmonic radiation of a helical undulator in synchrotron light sources. Originally, Sasaki & McNulty (2008) predicted that the  $n$ th-harmonic radiation from a helical undulator carried an OAM of  $\pm(n-1)\hbar$  per photon and that the sign of the OAM depended on the helicity of the radiation. This unique property of helical undulator radiation was first confirmed by Bahrtdt *et al.* (2013) for 99 eV photons, which corresponds to a wavelength of 12.5 nm, through an interference experiment at the BESSY-II storage



ring. Following these studies, optical vortex beams from helical undulators have been characterized experimentally at the UVSOR-III storage ring, mainly in the UV region and under diffraction-limited conditions (Sasaki *et al.*, 2015; Hosaka *et al.*, 2016; Katoh *et al.*, 2017b). Regarding the use of vortex beams, a photoionization study on rare gas atoms has been conducted in the extreme ultraviolet (XUV) region (Kaneyasu *et al.*, 2017). Since helical undulators are widely used in modern synchrotron light sources, the optical vortex beam generated as harmonic radiation from a helical undulator may open up new opportunities in synchrotron radiation research. To explore new applications of optical vortex beams, it is necessary to verify the vortical properties of harmonic radiation under a variety of operating conditions. In this paper, we report an interference experiment using two helical undulators, which allowed us to investigate the properties of optical vortex beams in the XUV region. In this experiment, the electron beam emittance was about four times larger than the diffraction-limited emittance. Although the interference patterns were slightly blurred owing to the relatively large electron beam emittance, it was possible to observe distinct interference features due to the helical wavefront of the vortex beam.

## 2. Experimental methods and setup

The experiment was carried out at the undulator beamline BL1U of the 750 MeV UVSOR-III storage ring. An optical vortex beam carrying an OAM of  $l\hbar$  ( $l = \pm 1$ ) per photon was produced as second-harmonic radiation from a helical undulator. To characterize experimentally the optical vortex beam, we observed an interference pattern between the optical vortex and a reference beam without OAM (Basistiy *et al.*, 1995; Vickers *et al.*, 2008; Bahrtdt *et al.*, 2013). Fig. 1 shows the experimental setup used for measuring the interference pattern between the photon beams from two helical (APPLE-II type) undulators. The period length and number of periods of the undulators were 88 mm and 10, respectively. The present interference experiment using two undulators followed the same approach as the BESSY-II experiment (Bahrtdt *et al.*, 2013) except for the polarization of the reference beam. In the present experiment, both undulators were set to produce circularly polarized radiation with the same

helicity in order to improve the visibility of the interference pattern relative to measurements with a horizontal linearly polarized reference beam. The improvement of the visibility is a result of both the horizontal and vertical field components of the circularly polarized reference beam interfering with the vortex beam.

The reference beam, which carries zero OAM, was produced as the fundamental radiation from the upstream undulator #1, while the optical vortex beam was produced as the second-harmonic radiation from the downstream undulator #2. The radiation wavelengths were tuned to 60 and 120 nm for the fundamental radiation from the upstream and downstream undulators, respectively. To perform the interference experiment, the electron beam orbit was adjusted so that the dark center of the optical vortex beam would coincide with the intensity maximum of the reference beam. In addition, the light pulses generated by the two undulators had to be stretched to achieve longitudinal overlap. As successfully demonstrated at BESSY-II (Bahrtdt *et al.*, 2013), this can be achieved by narrowing the bandwidth of undulator radiation with a monochromator. This method is analogous to the operation principle of the crossed undulator (Kim, 1984), which can produce variably polarized light based on the interference of light pulses from two undulators. We used a 0.2 m Seya-Namioka type monochromator equipped with a 2400 lines  $\text{mm}^{-1}$  grating. The bandwidth of the monochromator was set to 0.2 nm, which ensured a longitudinal overlap of  $\sim 90\%$ .

The spatial distribution of the photon beam was measured by scanning a pinhole in the transverse plane, as shown in Fig. 1. The 0.4 mm-diameter pinhole was located 8 m away from the center of the downstream undulator. The photon beam cut out by the pinhole was reflected and focused by pre-focusing mirror M0 into the entrance slit of the Seya-Namioka monochromator. After passing through the monochromator, the photon intensity was measured by a microchannel plate (MCP) located at the focal point of refocusing mirror M1. We did not use any optical elements that could distort the helical wavefront of the vortex beam before reaching the pinhole. An L-shaped slit was used to prevent stray light from entering the downstream section of the beamline.

The experiment was performed at a beam energy of 750 MeV with a beam current of 3 mA. The emittance of the

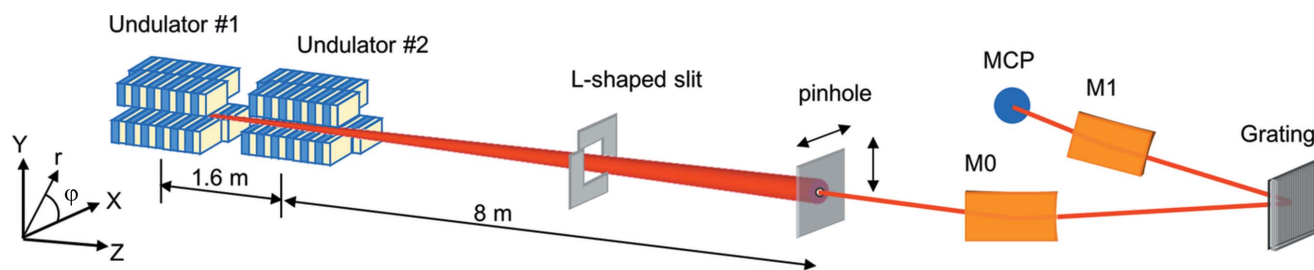
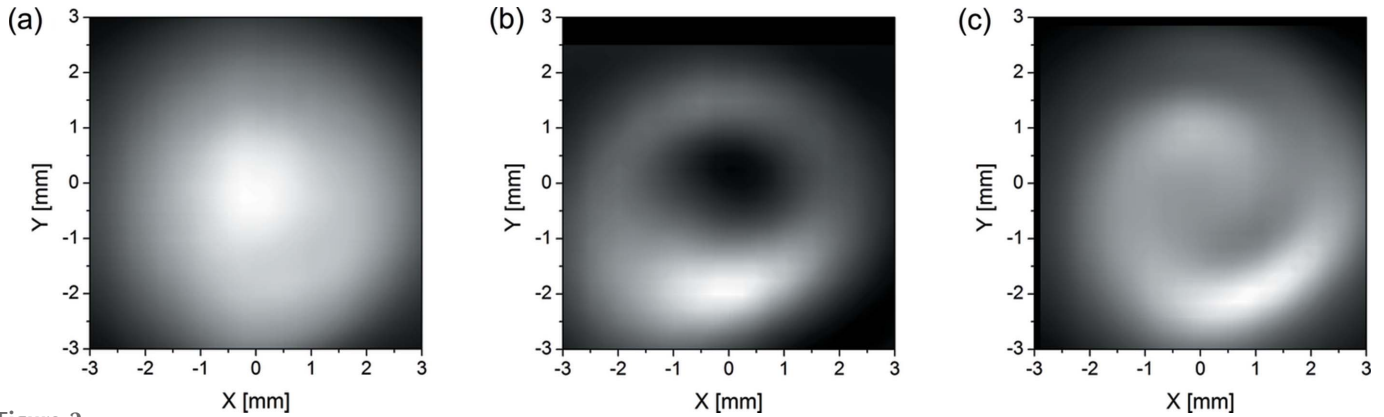


Figure 1

Experimental setup for measuring the interference pattern between the optical vortex and reference beams from two helical undulators in the XUV region. The reference beam with zero OAM was produced as the fundamental radiation of the upstream undulator #1, while the optical vortex beam was produced as the second-harmonic radiation of the downstream undulator #2. The photon beams from the undulators were monochromated by a 0.2 m Seya-Namioka monochromator. The intensity profile of the photon beam was measured by scanning a 0.4 mm-diameter pinhole. The throughput beam intensity was measured using a MCP.



**Figure 2** Spatial intensity distributions of right circularly polarized beams at 60 nm wavelength, measured by the pinhole scan in the transverse plane. Two-dimensional profiles for (a) fundamental radiation from the upstream undulator, (b) second-harmonic radiation from the downstream undulator, and (c) interference pattern.

electron beam was 17.5 nm rad, which is about four times the diffraction-limited emittance, 4.8 nm rad, at 60 nm wavelength.

### 3. Results and discussion

Fig. 2 shows the intensity profiles of photon beams measured for the individual undulators and the interference pattern between the two overlapping beams. In this measurement, both undulators were set to the right circular polarization (negative helicity) mode. We note that the circular polarization is defined from the viewpoint of the observer in this work. The fundamental radiation without OAM exhibits a Gaussian-like intensity distribution, while the second-harmonic radiation exhibits an annular distribution, which suggests the generation of the vortex beam. However, the helical wavefront of the vortex beam cannot be verified only by the intensity distribution; rather, it is necessary to utilize the interference method. As seen in Fig. 2(c), the interference pattern clearly exhibits a spiral structure due to the helical wavefront of the vortex beam. This spiral interference pattern is explained by the difference between the curvatures of the spherical helically phased beam and the spherical reference beam (Basistiy *et al.*, 1995). A counterclockwise rotation of the spiral pattern corresponds to a negative OAM, which depends on the helicity of radiation. To verify the longitudinal overlap between two photon beams, the intensity distributions on the horizontal and vertical central axes of the two-dimensional intensity profiles are compared in Fig. 3. Clearly, the intensity profiles of the overlapping beams are not reproduced by the incoherent sum of individual measurements, indicating that the interference condition between the two beams is satisfied.

Fig. 4(a) compares the interference patterns measured for the left and right circular polarization modes. The direction of the spiral pattern changes with the helicity, as predicted in theoretical studies (Sasaki & McNulty, 2008; Katoh *et al.*, 2017b). The spiral interference pattern is well described by a simple model assuming point sources (Bahrtdt *et al.*, 2013). We obtained the following analytical expression for the intensity

maximum of the interference pattern under our experimental conditions:

$$(n - 1)\varphi = \pm \left[ \frac{\pi d}{\gamma^2 \lambda} - \frac{\pi d}{L(L + d)\lambda} r^2 \right] + 2m\pi, \quad (1)$$

$$(m = 0, \pm 1, \pm 2, \dots),$$

where  $d$ ,  $\gamma$ ,  $\lambda$ ,  $L$ ,  $r$ ,  $n$  are, respectively, the distance between the centers of the two undulators, the Lorentz factor, wavelength

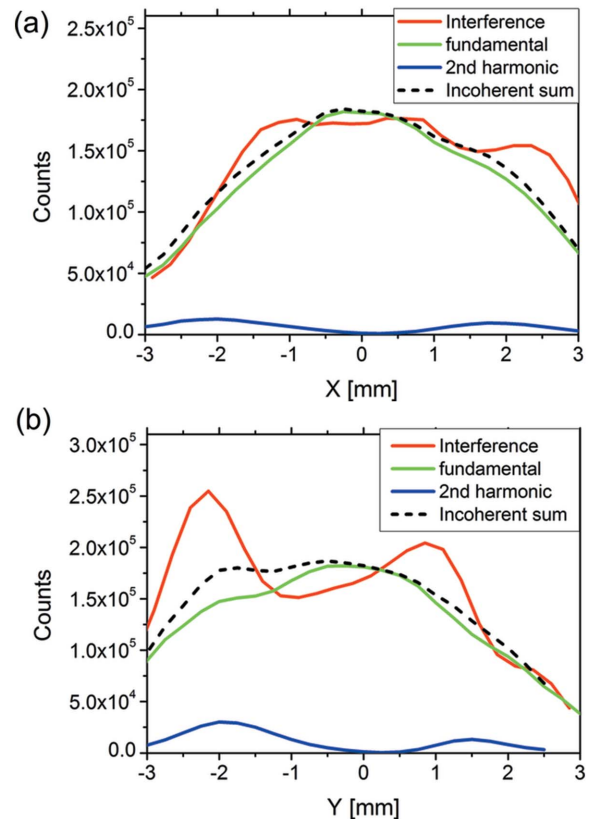


**Figure 3** Intensity profiles of photon beams at 60 nm wavelength, measured by the pinhole scan. The intensity profiles along the (a) horizontal and (b) vertical axes are derived from the two-dimensional distributions shown in Fig. 2.

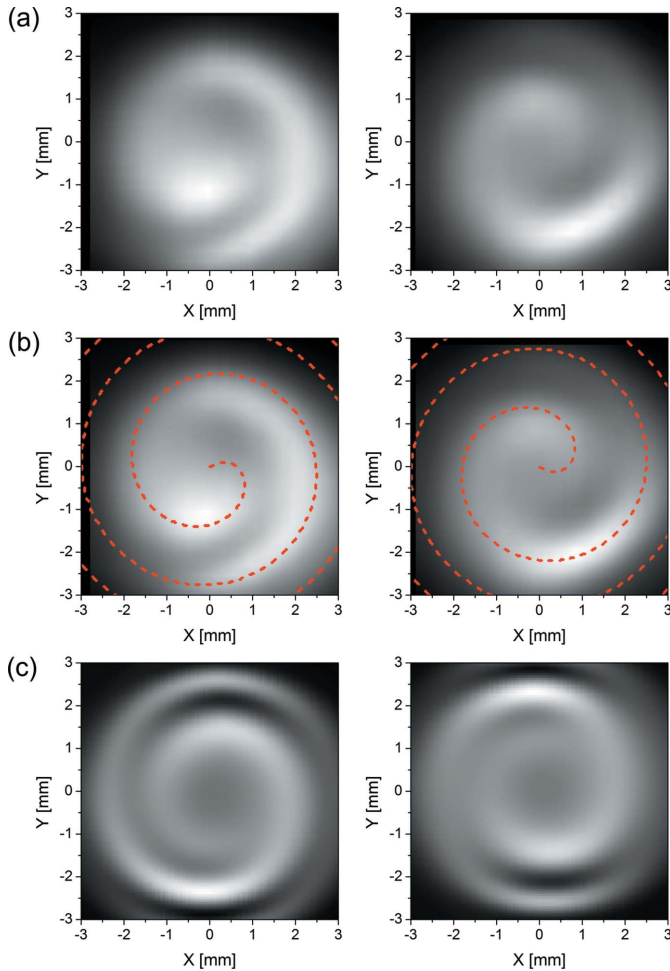


**Figure 4** Interference patterns at 60 nm wavelength produced by interfering the optical vortex beam with the reference beam without OAM. Left column: left circular polarization. Right column: right circular polarization. (a) Measurement results. (b) Same as (a) with the dotted curves representing the constructive interference patterns predicted by the theoretical model. The constant phase term of the theoretical model is adjusted to reproduce the measurements. (c) Simulation results by *SRW* code.

of light, distance between the center of the downstream undulator and the pinhole, radial distance, and harmonic number of the undulator radiation. The sign of the azimuthal angle corresponds to the helicity of the radiation. The vortex beam is emitted from the downstream undulator in our experiment, and the direction of the spiral pattern is the opposite of that obtained when the vortex beam is emitted from the upstream undulator (Bahrtdt *et al.*, 2013). This inversion of the spiral pattern depending on the source position is well understood in terms of the curvature of the spherical waves (Basistiy *et al.*, 1995). The dotted curves in Fig. 4(b) shows the calculated interference patterns obtained by equation (1), which agree with the experimental results for both polarization modes. Thus, it is reasonable to conclude that optical vortex beams carrying an OAM of  $l\hbar$  ( $l = \pm 1$ ) per photon are produced in the XUV region.

In the present experiment, the electron beam emittance is 17.5 nm rad, which is about four times larger than the

4.8 nm rad corresponding to the diffraction-limited emittance at 60 nm wavelength, in contrast to previous experiments (Bahrtdt *et al.*, 2013; Sasaki *et al.*, 2015; Hosaka *et al.*, 2016; Katoh *et al.*, 2017b) performed with a diffraction-limited or sufficiently small electron beam emittance. Consequently, the measured spiral patterns are blurred, owing to the relatively large electron beam emittance, whereas an individual electron emits an optical vortex with a phase singularity and zero-intensity minimum. This is essentially due to the incoherent overlap between the vortex radiation from individual electrons, and, when the emittance is increased, characterization of vortical properties becomes difficult because of blurring. To reveal the overall features of the interference pattern smeared by the finite emittance, we performed a simulation using the *SRW* code (Chubar *et al.*, 1999).

In this simulation, the horizontal emittance of the electron beam is taken into account, while the vertical emittance is neglected. This approximation is valid because of the relatively small vertical emittance resulting from the 5% coupling. To simplify the simulation, the interference pattern for a finite emittance is obtained as a superposition of the horizontally shifted interference pattern calculated for the zero-emittance case. For a finite emittance  $\varepsilon$ , the source position  $x$  and its angular divergence  $x'$  are repeatedly derived from random Gaussian distributions with standard deviations of, respectively,

$$\sigma_x = \left[ \beta\varepsilon + \eta^2 \left( \frac{\Delta E}{E} \right)^2 \right]^{1/2} \quad (2)$$

and

$$\sigma_{x'} = (\varepsilon/\beta)^{1/2}, \quad (3)$$

where  $\beta$  is the Twiss parameter,  $\eta$  is the dispersion function at the source point, and  $\Delta E/E$  is the energy spread of the electron beam. The simulation results are presented in Fig. 4(c). It can be clearly seen that the simulation reproduces the experiments, which confirms the reliability of the measurement. The visibility of the spiral patterns is slightly worse in the experiment than in the simulation. This is most likely due to the 0.4 mm-diameter pinhole, which is somewhat large for resolving the interference structure with sub-millimeter width.

To discuss the emittance effect on the interference pattern in more detail, we carried out further simulations under several conditions. Fig. 5 compares the simulation results obtained for 0, 17.5, 35, 87.5 and 175 nm rad emittances, which are 0, 1, 2, 5 and 10 times larger than the 17.5 nm rad emittance used in the experiment. The visibility of the spiral interference pattern is affected by the emittance, decreasing as the emittance is increased. Comparison of the simulation results reveals that at 17.5 nm rad the emittance effect is small enough to observe the interference pattern, as demonstrated in the present work. Furthermore, it may be possible to observe the spiral pattern at an emittance of 35 nm rad. In contrast, most of the spiral structure is smeared out at emittances larger than 87.5 nm rad, in which case it would be nearly impossible to verify the optical vortex beam by interference measurement.

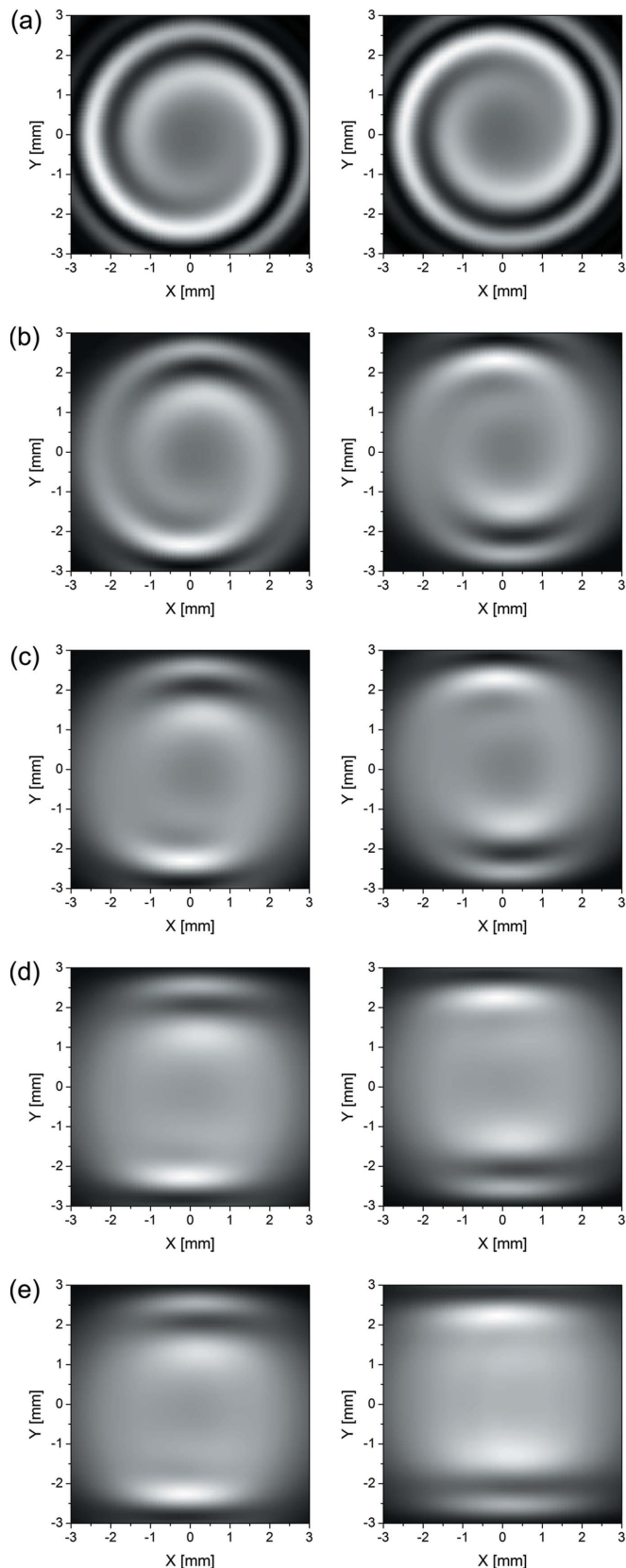


**Figure 5** Simulation of interference patterns between the fundamental and second-harmonic radiation at 60 nm wavelength. Left column: left circular polarization. Right column: right circular polarization. The interference patterns are calculated for emittances of (a) 0, (b) 17.5, (c) 35, (d) 87.5 and (e) 175 nm rad.

#### 4. Summary

We observed optical vortex beams at 60 nm wavelength using the interference method. The optical vortex beam carrying an OAM of  $l\hbar$  ( $l = \pm 1$ ) per photon was produced as the second-harmonic radiation from the helical undulator. Although the electron beam emittance was about four times larger than the diffraction-limited emittance, the vortical nature of the second-harmonic radiation was evident in the interference pattern. The measured interference patterns were in agreement with the theoretical curves and were well reproduced by the simulation. This work demonstrates the possibility of observation and characterization of optical vortex beams in a synchrotron light source, whose electron beam emittance is several times larger than the diffraction-limited emittance.

#### Acknowledgements

The authors acknowledge E. Nakamura and J. Yamazaki (IMS) for technical assistance. This work was supported by the Cooperative Research Program of the Institute for Molecular Science and Research Foundation for Opto-Science and Technology.

#### References

Allen, L., Beijersbergen, M. W., Spreeuw, R. J. C. & Woerdman, J. P. (1992). *Phys. Rev. A*, **45**, 8185–8189.

Bahrtdt, J., Holldack, K., Kuske, P., Müller, R., Scheer, M. & Schmid, P. (2013). *Phys. Rev. Lett.* **111**, 034801.

Basistiy, I. V., Soskin, M. S. & Vasnetsov, M. V. (1995). *Opt. Commun.* **119**, 604–612.

Beijersbergen, M. W., Coerwinkel, R. P. C., Kristensen, M. & Woerdman, J. P. (1994). *Opt. Commun.* **112**, 321–327.

Chubar, O., Elleaume, P. & Snigirev, A. (1999). *Nucl. Instrum. Methods Phys. Res. A*, **435**, 495–508.

Harwit, M. (2003). *Astrophys. J.* **597**, 1266–1270.

Heckenberg, N. R., McDuff, R., Smith, C. P. & White, A. G. (1992). *Opt. Lett.* **17**, 221–223.

Hell, S. (2003). *Nat. Biotechnol.* **21**, 1347–1355.

Hosaka, M., Miyamoto, K., Sasaki, S., Kuroda, K., Konomi, T., Yamamoto, N., Mirian, N. S. & Katoh, M. (2016). *Proceedings of the 7th International Particle Accelerator Conference (IPAC'2016)*, 8–13 May 2016, Busan, Korea, pp. 2036–2038.

Kaneyasu, T., Hikosaka, Y., Fujimoto, M., Konomi, T., Katoh, M., Iwayama, H. & Shigemasa, E. (2017). *Phys. Rev. A*, **95**, 023413.

Katoh, M., Fujimoto, M., Kawaguchi, H., Tsuchiya, K., Ohmi, K., Kaneyasu, T., Taira, Y., Hosaka, M., Mochihashi, A. & Takashima, Y. (2017a). *Phys. Rev. Lett.* **118**, 094801.

Katoh, M., Fujimoto, M., Mirian, N. S., Konomi, T., Taira, Y., Kaneyasu, T., Hosaka, M., Yamamoto, N., Mochihashi, A., Takashima, Y., Kuroda, K., Miyamoto, A., Miyamoto, S. & Sasaki, S. (2017b). *Sci. Rep.* **7**, 6130.

Kim, K. J. (1984). *Nucl. Instrum. Methods Phys. Res.* **219**, 425–429.

Marrucci, L., Manzo, C. & Paparo, D. (2006). *Phys. Rev. Lett.* **96**, 163905.

Omatsu, T., Chujo, K., Miyamoto, K., Okida, M., Nakamura, K., Aoki, N. & Morita, R. (2010). *Opt. Express*, **18**, 17967–17973.

Padgett, M. & Bowman, R. (2011). *Nat. Photon.* **5**, 343–348.

Sasaki, S. & McNulty, I. (2008). *Phys. Rev. Lett.* **100**, 124801.

Sasaki, S., Miyamoto, A., Hosaka, M., Yamamoto, N., Konomi, T. & Katoh, M. (2015). *Proceedings of the 6th International Particle Accelerator Conference (IPAC'15)*, 3–8 May 2015, Richmond, VA, USA, pp. 1563–1566.

Vickers, J., Burch, M., Vyas, R. & Singh, S. (2008). *J. Opt. Soc. Am. A*, **25**, 823–827.